INFLUENCE OF THE WELDING PARAMETERS ON THE HEAT AFFECTED ZONE FOR ALUMINUM WELDING

by

Jose L. MESEGUER-VALDENEBRO[c,d]*, Eusebio J. MARTINEZ-CONESA[b], Jose SERNA[a], and Antonio PORTOLES [c]

[a] University Center of Defence at the Spanish Air Force Academy, MDE-UPCT, Santiago de la Ribera, Spain
[b] Faculty of Architecture and Building Engineering. Technical University of Cartagena, Cartagena, Spain
[c] Department of Applied Physics and Materials Engineering, ESTII,
Technical University of Madrid, Madrid, Spain
[d] Inspection Department, Tecnicas Reunidas, Madrid, Spain

Original scientific paper
DOI:10.2298/TSCI140503106M

This work analyzes the heat affected zone in an aluminum alloy welded assembly using the metal inert gas welding technique. Making use of numerical simulations of the involved thermal processes, the aluminum alloy cooling curve is calculated and the extension of the heat affected zone is evaluated. The connection between this last parameter, the cooling rate, and the maximum obtained temperature is assessed. Additionally, the response surface method is exploited to fit the dependence of the heat affected zone with the welding parameters and to optimize these parameters in order to minimize that region.

Key words: *heat affected zone, aluminum welding, numerical simulation, cooling time, response surface method*

Introduction

The mechanical strength of welded joints in aluminum structures is a deeply studied topic in modern scientific literature [1]. The main objectives of these studies are the optimization of the designs [2] and the improvement of the structural behavior, being a typical example the aluminum bridges in civil engineering [3], whose historical evolution shows a continuous improvement in the joints design.

One of the exploited techniques for aluminum welding is the metal inert gas (MIG) welding technique. This is an electric arc welding process that makes use of a consumable welding wire and a shielding gas, usually argon. Recent studies on the MIG welding process, performed by the Schlieren visualization method [4] have shown that different qualities are obtained in the welded joints depending on the welding parameters, and the presence of surface defects such as pores, as a result of the shielding gas contamination. In view of these results, the optimization of the welding parameters is a concern in modern works in this field. As an example, it can be mentioned Schnick *et al.* [5] work, where a welding parameters optimization to improve the joint quality by reducing surface defects can be found.

In nowadays industrial environments, the design of metallic structures makes use of reference codes. In Europe, the most widespread code is the Eurocode [6] where the general guidelines for aluminum structures design and construction are defined. Regarding these structures, the code highlights the relevance of the heat affected zone (*HAZ*) [7], a region which is

* Corresponding author; e-mail: jlmeseguer@trsa.es; jlmeseguer507@gmail.com

not melted in the welding process but whose microstructure and properties are altered, and whose extension is clearly related to the mechanical properties of the joint. The key importance of the *HAZ* in welded joints is commonly found in other codes all around the world [8, 9].

The relevance of the *HAZ* in welded processes justifies the development of accurate numerical tools to study and predict this region. These numerical tools can be used, after validation with experimental results, to optimize the welding parameters in order to obtain the desired mechanical properties of the joint [7, 8]. This working methodology allows obtaining an economic saving as opposed to the classical empirical experiments, being only necessary a small amount of these experiments to validate the numerical method.

This work develops a numerical tool to analyze the effect of the welding parameters in an arc electric welded joint in the aluminum alloy 6063-T5, specifically their effect on the extension of the *HAZ*; afterwards, it is used to optimize the welding parameters.

Numerical model

Following a previous authors' work [10, 11] the 2-D heat equation is going to be used to determine the temperature field in MIG welding [12]. In particular, for an aluminum plate with uniform thickness, D, thermal conductivity, k, and heat capacity, C_p, (both temperature dependent [13]), density, ρ, and latent fusion heat, ΔH, the equation to determine the spatiotemporal temperature, T, evolution writes:

$$\frac{\partial T}{\partial t} = \frac{k}{\rho C_p}\left(\frac{\partial^2 T}{\partial x^2} + \frac{\partial^2 T}{\partial y^2}\right) + \frac{Q}{\rho C_p} \tag{1}$$

where heat transfer between the plate and the surrounding air due to convection, and heat losses at the plate edges are neglected. In this equation Q is a volumetric heat source that collects both the electric arc supplied heat and the heat due to phase change. The model considers that not all the electrical power (the product of the welding voltage, V, and the current intensity, I) can be used for the welding process, using a thermal efficiency factor, η [14]. Additionally the enthalpy variation due to phase changes is the product of the density and the latent heat ΔH_x, being x the liquid fraction. Considering that heat is liberated when a liquid to solid change occurs, the mathematical expression for Q is:

$$Q = \eta IV - \rho \Delta H_x \tag{2}$$

Finally, it is also worth mentioning that the model refines the implementation of the heat supplied by the electric arc by considering that it is spatially distributed in a double ellipsoidal geometry, a fact supported by several studies [13-17]. Details of the numerical description of this ellipsoid can be found in [11].

Numerical method

In order to solve eq. (1) with the appropriate boundary conditions, first order finite differences have been used for discretizing the spatial derivatives while Crank-Nicholson scheme is exploited for the temporal evolution. The details of the implementation in a similar problem (for stainless steel welding instead of aluminum welding) can be found in [11]. The numerical method has been implemented in the commercial software MATLAB R2011.

This method has been validated for a MIG process [19] where the influence that the *HAZ* has on a welded joint is determined.

Numerical experiments

In this work, the MIG welding technique is going to be considered to weld a 0.3 m × 0.075 m aluminum 6063-T5 plate with a thickness of 0.002 m. The filler material in the welding process will be the known as ER-4043, which exhibits thermal properties similar to those of the base material. The properties of the base and filler materials are in tab. 1.

Table 1. Properties of the aluminum alloy 6063-T5 [6] and ER-4043 [18, 19]

Parameter		6063-T5	ER-4043
Initial temperature [ºC]	T_o	20	20
Fourier conductivity [$Jm^{-1}s^{-1}K^{-1}$]	k	$0.07T + 190$	180
Fusion temperature [ºC]	T_f	654	630
Heat capacity [$Jkg^{-1}K^{-1}$]	C_p	$0.41T + 903$	850
Density [kgm^{-3}]	ρ	2700	2690
Phase change enthalpy [Jkg^{-1}]	ΔH	9000	8700

The response surface methodology

Taking into account that the main objective of this work is the optimization of the *HAZ*, a short introduction to the chosen optimization procedure must be done. In this case, the response surface methodology (RSM) is exploited. This method allows the optimization of a response function subject to different independent variables after modelling the influence of these variables with a minimum number of experiments. To do so a sequential strategy is carried out in order to obtain the maximum amount of information with the minimum effort.

From a certain number of experiments, the variables which influence the response are determined. Once these variables have been identified, an estimative of the response surface is obtained by means of factorial models. This response surface is used as a reference to gradually vary the factors affecting the response, in order to improve their values.

In this study, second-order polynomial expressions are going to be used, due to their simplicity and ability to model the effects under study. The general formulation for these response surfaces is:

$$y = \beta_0 + \sum_{i=1}^{k} \beta_i x_i + \sum_{i=1}^{k} \beta_{ii} x_i^2 + \sum_{j=2} \sum_{i=1}^{k} \beta_{ij} x_i x_j (i < j) + \varepsilon \tag{3}$$

where ε is the experimental error, x_1, x_2, …, x_k – the independent variables, and β_0, β_1,…, β_k – the regression coefficients of the surface calculated from the experimental data.

As shown later, the power, P, the welding efficiency, η, and the welding velocity, v_s, will be the scanned parameters that have influence on the *HAZ*. Thus, the expression for the RSM related to this formulation is:

$$HAZ_{\mathrm{RSM}} = \beta_0 + P\beta_1 + v_s\beta_2 + \eta\beta_3 + Pv_s\beta_4 + P\eta\beta_5 + v_s\eta\beta_6 + P^2\beta_7 + v_s^2\beta_8 + \eta^2\beta_9 \tag{4}$$

Design of experiments

The design of experiments, an essential point in the RSM, is performed through three steps [20-23]:

(1) Identify the parameters of the process. In this case, the parameters which have been taken into account to carry out the experiments are: power, welding velocity, and welding efficiency.
(2) Define the ranges of variation of the parameters (levels). For aluminum MIG welding, the electric inputs of the welding range from 100-130 A for the intensity, and from 18 to 22 V for the voltage. With these values, the input power varies from 1800-2860 W. The parameters values, considering three levels for each parameter, are collected in tab. 2.
(3) Define the matrix of experiments. The matrix of performed experiments establishes the relationship between the welding process variables and the three levels of the system, as indicated in tab. 3.

Table 2. Levels of the MIG welding for Al 6063-T5 process variables

Parameter		Levels		
		-1	0	1
Power, [W]	P	1800	2330	2860
Welding velocity, [ms^{-1}]	v_s	10	11,5	13
Welding efficiency [–]	η	0,7	0,775	0,85

Table. 3. Matrix of experiments

Experiment	Design matrix			Intensity, [A]	Voltage, [V]	P, [W]	$v_s \cdot 10^{-3}$, [ms^{-1}]	η
1	–1	–1	0	100	18	1800	10	0,7750
2	–1	1	0	100	18	1800	13	0,7750
3	1	–1	0	130	22	2860	10	0,7750
4	1	1	0	130	22	2860	13	0,7750
5	–1	0	–1	100	18	1800	11,5	0,7
6	–1	0	1	100	18	1800	11,5	0,85
7	1	0	–1	130	22	2860	11,5	0,7
8	1	0	1	130	22	2860	11,5	0,85
9	0	–1	–1	116,5	20	2330	10	0,7
10	0	–1	1	116,5	20	2330	10	0,85
11	0	1	–1	116,5	20	2330	13	0,7
12	0	1	1	116,5	20	2330	13	0,85
13	0	0	0	116,5	20	2330	11,5	0,7750
14	0	0	0	116,5	20	2330	11,5	0,7750
15	0	0	0	116,5	20	2330	11,5	0,7750

Results and discussion

Calculation of the HAZ

As shown in tab. 3, fifteen numerical experiments are going to be performed to get a functional dependence of the *HAZ* with the welding parameters, making use of the RSM. Fig-

ure 1 shows the temperature distributions at a given time for the studied experiments, being the co-ordinate axis the spatial directions. As later explained, the accurate determination of the temperature field is the essential step to characterize the *HAZ*.

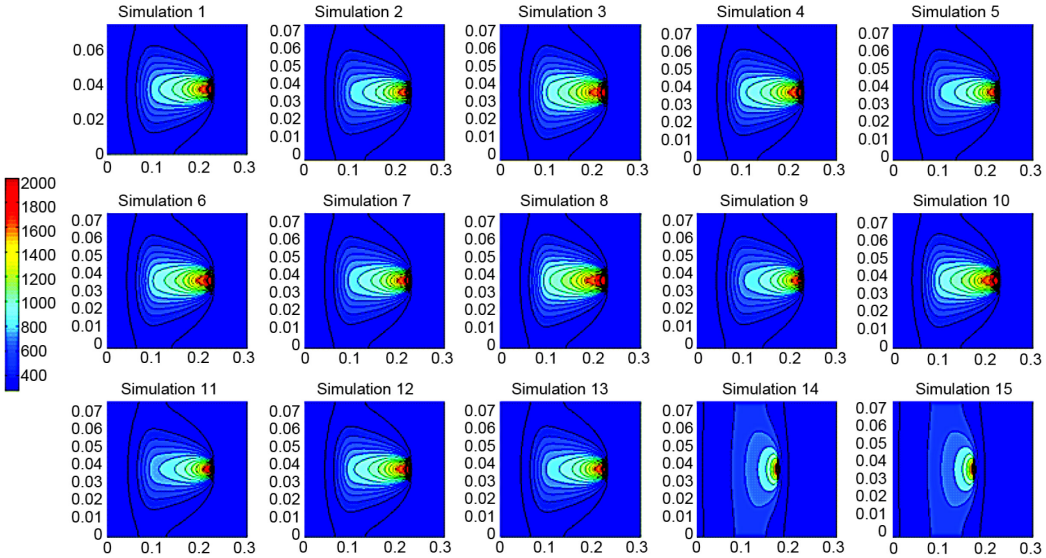

Figure 1. Temperature fields at a given time obtained from numerical simulations. Legend is ºC
(for color image see journal web-site)

As expected, fig. 1 shows that highest temperature values are found in the center of the generated weld bead (the zone in direct contact with the electrode), exhibiting a decay towards the edges of the plate. The temperature field for experiment 1 is shown in fig. 2 to clarify the extension of the region affected by high temperatures. According to [24], the *HAZ* for the material under study is the region where temperatures above 400 ºC are reached. In this zone, structural changes in the aluminum and a variation in the mechanical properties can be appreciated. Taking into account this criterion, the size of the *HAZ* has been calculated as the distance from the center of the weld bead to the point where 400 ºC is reached, in the direction orthogonal to the moving electrode path, *i. e.*, because the electrode path is the x-axis in figs. 1 and 2, the distance is measured along the y-axis. The numerical results for the different experiments are collected in tab. 4.

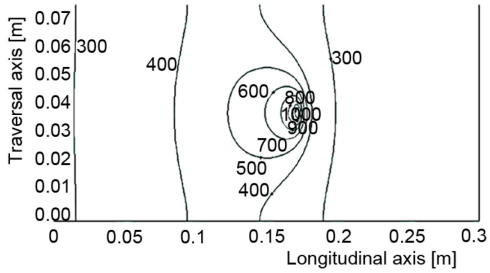

Figure. 2. Temperature field in simulation 1. The contours values are ºC

Evaluation of the cooling time and the cooling rate

To characterize the cooling process in the welded joint, the temporal evolution of the temperature in a point placed in the center line of the plate (starting just after the electrode has gone by) has been monitored. The evolution of this parameter for the performed experiments

Table 4. Results of the *HAZ* obtained for each of the experiments

Experiment	P, [W]	$v_s \cdot 10^{-3}$, [ms^{-1}]	η	HAZ, [mm]
1	1800	10	0,7750	6
2	1800	13	0,7750	4,5
3	2860	10	0,7750	13,5
4	2860	13	0,7750	10,5
5	1800	11,5	0,7	4,5
6	1800	11,5	0,85	7,5
7	2860	11,5	0,7	10,5
8	2860	11,5	0,85	13,5
9	2330	10	0,7	9
10	2330	10	0,85	12
11	2330	13	0,7	7,5
12	2330	13	0,85	9
13	2330	11,5	0,7750	9
14	2330	11,5	0,7750	9
15	2330	11,5	0,7750	9

is collected in fig. 3, where the abscissas axis represents the cooling time and the ordinate represents the temperature evolution. It can be seen, that a dependence of the cooling time with the welding parameters exists.

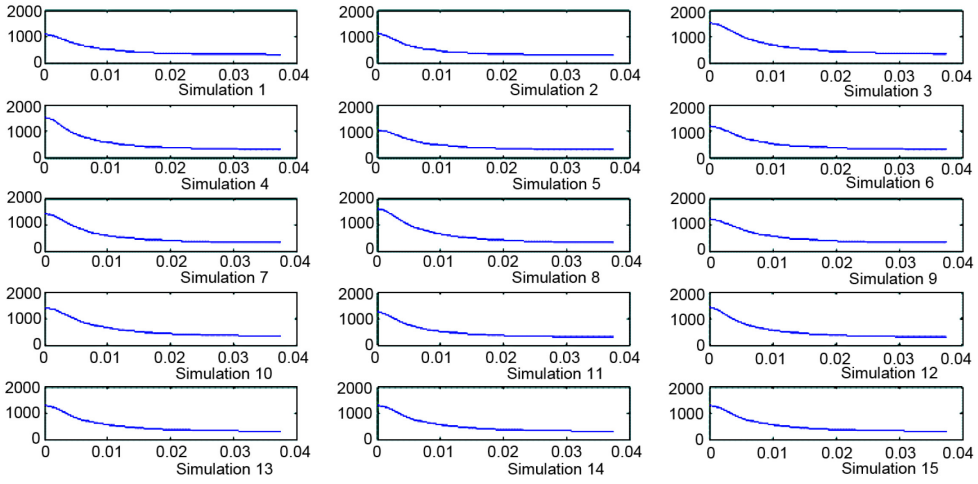

Figure 3. Cooling curves obtained from numerical experiments: x-axis: cooling time, y-axis: temperature [ºC]

From the calculated cooling curves, the rate of temperature variation can be evaluated by means of numerical derivatives. In this case, a first order numerical scheme has been used to evaluate this rate of temperature decay or cooling rate, which is shown in fig. 4.

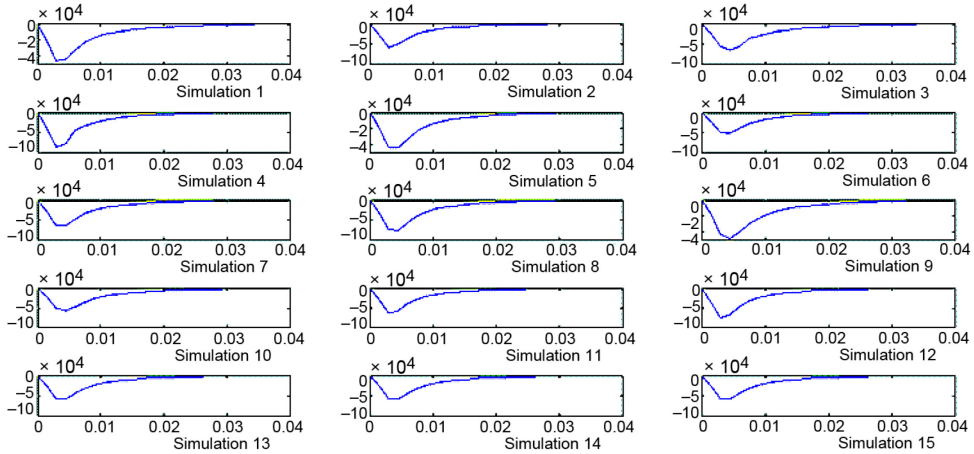

Figure. 4. Rate of variation of temperature during cooling: x-axis: cooling time, y-axis: cooling rate d*T*/d*t*

Connection between the HAZ and the cooling rate

Once the *HAZ* and the cooling rate have been evaluated, a connection between these two parameters can be sought. Table 5 collects the numerical values obtained for the size of the *HAZ* calculated by the numerical method and the maximum cooling rate, this information is shown graphically in fig. 5.

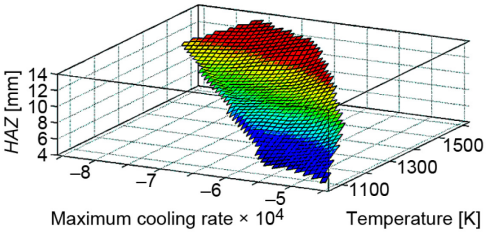

Figure 5. Surface representation of the connection between maximum cooling rate and the maximum temperature with the size of the *HAZ* *(for color image see journal web-site)*

In fig. 5, it can be verified that as the maximum cooling rate and/or the maximum temperature increases, the size of the *HAZ* also increases. This fact proves the *HAZ* is increased if the cooling times are slow and the process temperatures are high.

Table 5. Size of the *HAZ*, maximum temperature, and maximum cooling rate obtained from numerical simulations

Experiment	*HAZ* [mm]	Maximum temperature [10^3 K]	Maximum cooling rate [104 Ks^{-1}]
1	6	1.0920	–4.5949
2	4,5	1.1287	–5.7581
3	13,5	1.5323	–6.3492
4	10,5	1.5440	–8.5866
5	4,5	1.0466	–4.4306
6	7,5	1.2081	–5.1701
7	10,5	1.4417	–6.5157
8	13,5	1.6288	–7.6502
9	9	1.2194	–4.7985
10	12	1.4080	–5.6920
11	7,5	1.2619	–6.3927
12	9	1.4326	–7.5176
13	9	1.3087	–5.7923
14	9	1.3087	–5.7923
15	9	1.3087	–5.7923

The RSM applied to the HAZ

Table. 6. Adjust to the *HAZ* to the regression model in eq. (4). Regression coefficients, numerically obtained *HAZ*, *HAZ* calculated from the regression model, and residues

Regression coefficients		Experiment	*HAZ* exp., (mm)	*HAZ* – *RSM*, (mm)	Residue, (mm)
β_0	19,2795	1	06,53	06,00	–0,538
β_1	0,012	2	04,42	04,50	0,071
β_2	335,3284	3	12,96	13,50	0,538
β_3	–93,3261	4	10,57	10,50	0,071
β_4	0,0270	5	04,23	04,50	0,264
β_5	0	6	07,29	07,50	0,203
β_6	904,6505	7	10,70	10,50	–0,203
β_7	0	8	13,76	13,50	–0,264
β_8	$-8.6013 \cdot 10^4$	9	09,07	09,00	–0,071
β_9	66,6667	10	11,92	12,00	0,071
		11	07,49	07,50	0,009
		12	09,00	09,00	–0,009
		13	09,00	09,00	0,000
		14	09,00	09,00	0,000
		15	09,00	09,00	0,000

The polynomial coefficients in eq. (3), calculated with a multivariable regression from the numerical experiments, are shown in tab. 6. In order to manifest the goodness of the fitting, the values of both the *HAZ* calculated from the numerical experiments and from the regression expression are also collected in tab. 6. These data are pictured in the dispersion diagram in fig. 6 to give a visual representation of the goodness of the analysis.

To complete the regression analysis, ANOVA procedures have been used [25]. The fitness curves are shown in fig. 7. These curves exhibit R^2 = 99,24% and R^2_{fitted} = = 97,87%. It is observed that both curves have a very similar trajectory and the dispersion values are also quite similar, which indicates the existence of a very close relationship between both fits.

In tab. 7 the *F*-quotient and its level of significance or *p*-value are shown. The level

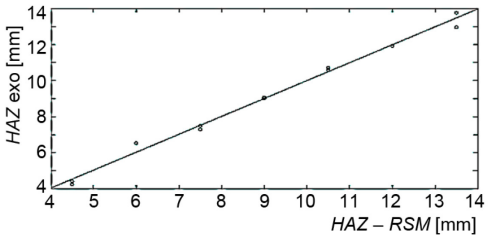

Figure 6. Dispersion diagram for the values of the *HAZ*

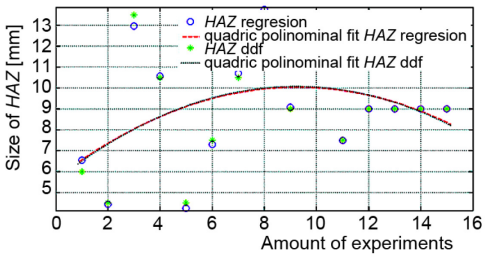

Figure 7. Fitness curve of the *HAZ* calculated statistically and of the *HAZ* calculated computationally

of significance allows us to accept or reject the null hypothesis, *i. e.*, the independence between input variables, without making use of statistical tables of the Snedecor distribution function. In the case under study, the *p*-value is $9.2066 \cdot 10^{-6}$, a small enough value to justify the viability of the model presented in eq. (4).

Table 7. Variance analysis. ANOVA table

Variance analysis	Degrees of freedom	Sum of squares	Mean of squares	*F*-quotient	*p*-value
Columns	5	107,1790	11,9092	72,5287	$9,2066 \cdot 10^{-6}$
Error	9	0,8210	0,1642		
Total	14	108	12,0734		

Analysis of the response surfaces

The response surfaces collect the influence that the input variables, *i. e.* the welding velocity, the thermal efficiency, and the supplied electrical power, have on the output variable, in this case, the size of the *HAZ*. In fig. 8 the response surfaces obtained for the regression model are shown in order to study the effect of the different studied welding parameters.

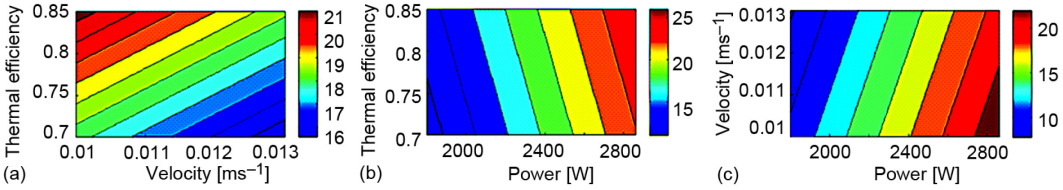

Figure 8. Response surfaces for the *HAZ* [mm] with: (a) power [W] – velocity [ms^{-1}] for $\eta = 0.75$, (b) thermal efficiency [–] – power [W] for $v = 5$ m/s; (c) velocity [ms^{-1}] – thermal efficiency [–] for $P = 2500$ W *(for color image see journal web-site)*

Figures 8(a) and 8(c) indicate that as the velocity increases, for fixed power and thermal efficiency, the *HAZ* decreases. Nevertheless, an increase in the thermal efficiency, figs. 8(b) and 8(c), or in the supplied electrical power, figs. 8(a) and 8(b), translates into an increase of the *HAZ* region. This is the expected behavior and the proposed regression model allows a quantification of the different effects.

The HAZ optimization

In any welded joint, the *HAZ* minimization as far as possible is a key objective. For that reason, once the regression model between the *HAZ* and the welding parameters has been obtained, an optimization procedure has been performed. To do that, the MATLAB response optimizer has been exploited. This software provides an optimum solution for the combinations of input variables by means of a graphical interface [25] Considering an acceptable average value of the *HAZ* of 9 ± 0,56 mm [26] the optimum values for the input variables are: $P = 2330$ W, $v_s = 0.00806 \cdot 10^{-3}$ m/s, and $\eta = 0{,}775$. The output from the optimizer for this case is shown is fig. 9, where "□" symbol lines represent the confidence intervals, and "o" symbol dotted lines represent the evolution of every variable in relation to the size of the *HAZ*.

Conclusions

In this work a numerical simulation tool has been developed to study the temperature field in aluminum welding with the MIG technique. The numerical experiments, per-

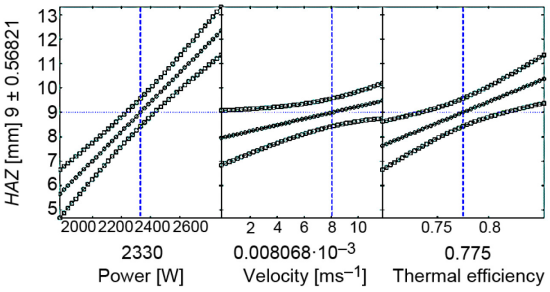

Figure 9. Optimized parameters obtained from the *HAZ* model (graphical interface output)

formed for the 6063-T5 aluminum alloy, allow the determination of the *HAZ*, the maximum obtained temperature, and the cooling rates as functions of welding input parameters (supplied electrical power, welding velocity, and welding efficiency) typical for MIG welding. It is found that, in general, the greater temperature and lower cooling rate, the larger *HAZ*.

The simulations results are used to obtain an engineering law for the dependence of the *HAZ* with the input parameters and the RSM is exploited to characterize the effects of these parameters on the *HAZ* and to optimize it. As expected, the most energy supplied per surface unit (proportional to the supplied electrical power and welding efficiency, and inversely proportional to the welding velocity) originates the largest *HAZ*. This study allows a quantification of these effects for the studied aluminum allow and welding technique.

Finally, the fitted model based on a reduced number of parameters and which goodness is assessed, is used to optimize the welding parameters in order to obtain a reduced *HAZ*. This results is of great interest for the optimization of several industrial processes.

Nomenclature

C_p – heat capacity, [Jkg^{-1}K^{-1}]
D – thickness of the aluminium 6063-T5 plate to be simulated, [m]
ΔH – phase change enthalpy, [Jkg^{-1}]
k – thermal conductivity, [Jm^{-1}s^{-1}K^{-1}]
P – power of the electric arc, [W]
T_o – initial temperature, [ºC]
T_f – fusion temperature, [ºC]
v_s – welding speed, [ms^{-1}]
x_i – independent variables
y – response surface

Greek symbols

β – regression parameters of the surface estimated from experimental data
ε – experimental error
η – thermal efficiency
ρ – density, [kgm^{-3}]

Acronyms

ANOVA – Variance analysis
RSM – response surface methodology
MIG – metal inert gas
HAZ – heat affected zone

References

[1] Oluwole, O. I., Ajibade, O. J., Effect of Welding Current and Voltage on the Mechanical Properties of Wrought (6063) Aluminium Alloy, *Materials Research-Ibero-American Journal of Materials*, *13* (2010), 2, pp. 125-128
[2] Miguel, V., *et al.*, Optimization of GMAW Process of AA 6063-T5 Aluminum Alloy Butt Joints Based on the Response Surface Methodology and on the Bead Geometry, *Revista de Metalurgia*, *48* (2012), 5, pp. 333-350
[3] Saleem, M. A., *et al.*, Experimental Evaluation of Aluminum Bridge Deck System, *Journal of Bridge Engineering*, *17* (2012), 1, pp. 97-106
[4] Siewert, E., *et al.*, Visualization of Gas Flows in Welding Arcs by the Schlieren Measuring Technique, *Welding Journal*, *93* (2014), 1, p. S1-S5
[5] Schnick, M., *et al.*, Visualization and Optimization of Shielding Gas Flows in Arc Welding, *Welding in the World*, *56* (2012), 1-2, pp. 54-61

[6] ***, CEN Technical Committee, Eurocode 9: Design of Aluminium Structures. Part 1-1. General Rules, BSI, 2009
[7] Mitrović, R. M., *et al.*, Study on Impact Properties of Creep-Resistant Steel Thermally Simulated Heat Affected Zone, *Thermal Science*, *16* (2012), 2, pp. 513-525
[8] Madić, M. J., Radovanović, M. R., Analysis of the Heat Affected Zone in CO_2 Laser Cutting of Stainless Steel, *Thermal Science*, *16* (2012), Suppl. 2, pp. S363-S373
[9] Lazić, V. N., *et al.*, Theoretical-Experimental Determining of Cooling Time (T(8/5)) in Hard Facing of Steels for Forging Dies, *Thermal Science*, *14* (2010), 1, pp. 235-246
[10] Coniglio, N., Patry, M., Measuring Laser Weldability of Aluminium Alloys Using Controlled Restraint Weldability Test, *Science and Technology of Welding and Joining*, *18* (2013), 7, pp. 573-580
[11] Meseguer-Valdenebro, J. L., *et al.,* Calculation of t8/5 by Response Surface Methodology for Electric Arc Welding Applications, *Thermal Science*, *18* (2014), Suppl. 1, pp. S149-S158
[12] Al-Saady, M. H., *et al.*, Finite Difference Simulation of Low Carbon Steel Manual Arc Welding, *Thermal Science*, *15* (2011), 1, pp. 207-214
[13] Leister, B. M., DuPont, J. N., Fracture Toughness of Simulated Heat Affected Zones in Nucu-140 Steel, *Welding Journal*, *91* (2012), 2, p. 53s-58s
[14] Vrouwenvelder, T., *et al.*, Modelling of *HAZ*ards, *Structural Engineering International*, *22* (2012), 1, pp. 73-78
[15] Arora, H. S., *et al.*, Numerical Simulation of Temperature Distribution Using Finite Difference Equations and Estimation of the Grain Size During Friction Stir Processing, *Materials Science and Engineering, A – Structural Materials Properties Microstructure and Processing*, *543* (2012), May, pp. 231-242
[16] Estrems Amestoy, M., *et al.*, Numerical Development for Obtaining the Temperature Field in Stainless Steels Arc Welding Processes, *Dyna*, *84* (2009), 9, pp. 1-8
[17] Ho, C. Y., Lee, Y. C., Temperature Fields in the Fusion Zone Induced by a Moving Electron Beam, *Journal of Mechanical Science and Technology*, *21* (2007), 10, pp. 1707-1713
[18] Guo, Z., *et al.*, Numerical Simulation of Temperature Field for TIG Welding of Aluminum Alloy Sheet Based on the SYSWELD, *LAUBLSRUTISTR 24*, CH-8717 Stafa-Zurich, Zurich, Switzerland, 2012, pp. 472-475, pp. 1945-1949
[19] Nguyen, N. T. *et al.*, A Analytical Approximate Solution for Double Ellipsoidal Heat Source in Finite Thick Plate, *Welding Journal*, *83* (2004), 3, pp. 82s-93s
[20] Coniglio, N., *et al.*, Phase Formation in 6060/4043 Aluminum Weld Solidification, *Materials Science and Engineering: A*, *517* (2009), 1-2, pp. 321-327
[21] Totten, G. E., MacKenzie, D. S., *Handbook of Aluminum: Physical Metallurgy and Process*, Marcel Dekker, New York, USA, 2003
[22] Montgomery, C., Myers, R. H., *Response Surface Methodology: Process and Product in Optimization Using Designed Experiments*, John Wiley & Sons, New York, USA, 1995
[23] Allen, T. T., *Introduction to Engineering Statistics and Six Sigma*, Springer, London, 2006
[24] Ivanović, I. B., *et al.*, Numerical Study of Transient Three-Dimensional Heat Conduction Problem with a Moving Heat Source, *Thermal Science*, *15* (2011), 1, pp. 257-266
[25] ***, M. U. Guide, MathWorks, Inc., Natick, Mass, USA, Vol. 5, 1998
[26] Brungrab, R. J., Nelson, F., Effect of Welding Variables on Aluminum-Alloy Weldments, *Welding Journal*, *52* (1973), 3, pp. S97-S103

Paper submitted: May 3, 2014
Paper revised: July 3, 2014
Paper accepted: August 17, 2014